Author's Accepted Manuscript

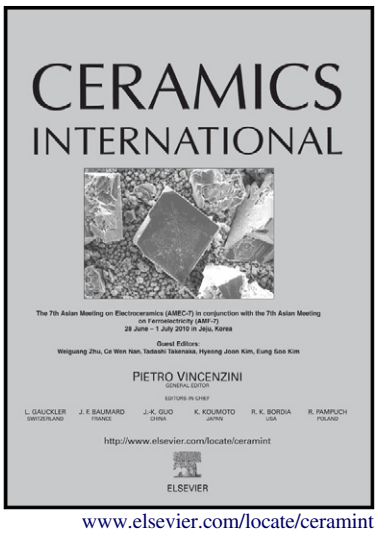

www.elsevier.com/locate/ceramint

Effect of titania addition on the properties of freeze-cast alumina samples

Alysson M.A. Silva, Eduardo H.M. Nunes, Douglas F. Souza, Dana L. Martens, João C. Diniz da Costa, Manuel Houmard, Wander L. Vasconcelos

PII: S0272-8842(15)00888-3
DOI: http://dx.doi.org/10.1016/j.ceramint.2015.04.132
Reference: CERI10539

To appear in: *Ceramics International*

Received date: 31 March 2015
Accepted date: 23 April 2015

Cite this article as: Alysson M.A. Silva, Eduardo H.M. Nunes, Douglas F. Souza, Dana L. Martens, João C. Diniz da Costa, Manuel Houmard, Wander L. Vasconcelos, Effect of titania addition on the properties of freeze-cast alumina samples, *Ceramics International,* http://dx.doi.org/10.1016/j.ceramint.2015.04.132

EFFECT OF TITANIA ADDITION ON THE PROPERTIES OF FREEZE-CAST ALUMINA SAMPLES

Alysson M.A. Silva[(1)*], Eduardo H.M. Nunes[(1)**], Douglas F. Souza[(1)], Dana L. Martens[(2)], João C. Diniz da Costa[(2)], Manuel Houmard[(3)], Wander L. Vasconcelos[(1)***]

(1) Department of Metallurgical and Materials Engineering,

Federal University of Minas Gerais – UFMG

Avenida Presidente Antônio Carlos, 6627, Campus UFMG, Belo Horizonte, MG,

CEP: 31270-901, Escola de Engenharia, bloco 2, sala 2230 – Brasil

(2) The University of Queensland, FIM^{2}Lab – Functional and Interfacial Materials and Membranes Laboratory, School of Chemical Engineering, Brisbane, Queensland, 4072, Australia

(3) Department of Materials Engineering and Civil Construction,

Federal University of Minas Gerais – UFMG

Avenida Presidente Antônio Carlos, 6627, Campus UFMG, Belo Horizonte, MG,

CEP: 31270-901, Escola de Engenharia, bloco 1, sala 3304 – Brasil

* alysson_fisica@yahoo.com.br

** eduardohmn@gmail.com

*** wlv@demet.ufmg.br

ABSTRACT

This work investigated the behavior of TiO_2-containing α-Al_2O_3 samples prepared by the freeze-casting technique. Camphene and liquid nitrogen were used as the solvent and cooling fluid, respectively. Camphene resulted in the formation of dendritic pores, in the direction of the freeze-casting cold front during sample preparation. The formation of β-Al_2TiO_5 phase occurred at 1300 °C, and became more evident as the sintering temperatures reached 1500 °C. The TiO_2 loading did not affect the sample porosity at a given temperature, but it was detrimental in the case of mechanical properties under certain conditions. For instance, the flexural strength slightly improved with increasing the TiO_2 loading and sintering temperature from 1100 to 1300 °C. This effect was attributed to the occurrence of a more effective sintering of alumina. However, as the heat treatment temperature was raised from 1300 to 1500 °C, the flexural strength did not increase as a function of the TiO_2 loading, even though the densification occurred with loss of porosity. The loss of mechanical strength was found to be associated with the formation of microcracks which stemmed from the formation of β-Al_2TiO_5 phase for TiO_2 loadings in excess of 4 wt% at these high sintering temperatures.

KEYWORDS: B. Porosity; D. Al_2O_3; D. TiO_2; D. Al_2TiO_5.

1. INTRODUCTION

A number of processing techniques have been developed for decades for preparing porous ceramic materials. These include, among others, the replication of polymer foams by impregnation [1, 2], foaming of aqueous powder suspensions [3, 4], pyrolysis of pre-ceramic precursors [5, 6], and heating of powder compacts with pore-forming sacrificial templates [7, 8]. However, these methods cannot completely satisfy a controlled level of interconnected porosity combined with an outstanding mechanical strength. An alternative approach is to use the freeze-casting technique to obtain porous ceramic samples.

Freeze-casting is a versatile route for preparing ceramic materials with tailored pore structures [9]. It is an environmentally friendly, cost effective, and easy to scale-up method. This preparation technique consists of a stable colloidal suspension of ceramic particles which is poured into a mold, freezing the suspension, removing the dispersing medium, and sintering the obtained material. In this methodology the slurry particles are pushed away by the solidification front and trapped between the growing crystals [10]. Freeze-cast samples usually show an improved mechanical strength and a highly interconnected three-dimensional pore network [11]. This behavior can provide to these materials an enhanced fluid permeability and chemical stability [12, 13]. Freeze-cast materials have been used in a range of applications, including biomaterials [14, 15], sensors [16, 17], drug delivery systems [18, 19], photocatalysis [20, 21], and gas purification [22-24].

The addition of titania into alumina has been widely investigated for a variety of applications, including catalysts and mechanically reliable ceramics [25-28]. It is well established that the formation of an aluminum titanate (Al_2TiO_5) phase can increase the thermal shock resistance and mechanical strength of alumina [29-31]. In this work we investigate TiO_2-containing α-Al_2O_3 samples prepared by the freeze-casting technique. As far as we know, this is the first attempt to incorporate titania into freeze-cast alumina, thus allowing the examination of novel tailored pore structures coupled with mechanical properties. This study is supported by a series of experimental tests including X-ray diffraction (XRD), Fourier transform infrared spectroscopy (FTIR), Scanning electron microscopy (SEM), Archimedes method, X-ray microtomography (μ-CT), and mechanical tests using a stage available in the μ-CT system.

2. MATERIALS AND METHODS

2.1 SYNTHESIS

Figure 1 depicts a schematic of the steps used in this work for samples preparation. Initially a solution of Texaphor 963 (Cognis, Southampton Hampshire, UK) and camphene (Aldrich / ≥ 95%) was prepared at 60 °C. CT3000SG alumina particles (Almatis, Brazil) with a mean diameter of 1 μm and 99.8 % purity were added under vigorous stirring to the solution. The as-prepared slurry was kept under sonication for 15 min. Titania (Sigma / 325 mesh anatase / ≥ 99%) was then added to the slurry. The titania loading in the prepared slurries ranged from 1 to 14 wt% of the solid concentration. Blank samples containing pure alumina were also prepared for

comparison purposes. The Texaphor 963 loading was kept at 1.8 wt% of the alumina concentration. The ceramic concentration in the obtained slurries was kept at 25 vol%. Subsequently, the slurries were poured into Polytetrafluorethylene (PTFE) molds as shown in Figure 1. The molds were placed on a high thermal conductivity copper plate. The top side of the mold was open so that the slurry surface was kept under atmospheric conditions. As a result, the camphene crystals obtained during the freezing step were stimulated to grow in the vertical orientation from the bottom to the top side. Liquid nitrogen was used as the cooling fluid. The sublimation of camphene was performed by keeping samples in air at room temperature for at least 3 days. Then, the materials were heat treated in air at 1100, 1300 or 1500 °C using a temperature-controlled Thermolab furnace (Pt30%Rh/Pt6%Rh-thermocouple) at a heating rate of 2 °C min^{-1}. The sintering time was kept constant at 2 h.

2.2 CHARACTERIZATION

The porosity of the sintered samples was assessed by the Archimedes method. The samples shrinkage was evaluated taking into account their diameter before and after the heat treatment step. XRD was carried out using a PHILIPS-PANALYTICAL PW 1710 diffractometer, with Cu Kα radiation and operating at 40 kV and 30 mA. XRD patterns were taken in the range of 10-80 ° (2θ), using a step size of 0.06 °. The identification of the crystalline phases was performed using the XPert Plus software. FTIR was performed using samples prepared as pellets with KBr and examined in a PERKIN-ELMER Frontier spectrometer. The spectra were taken from 4000 to 400 cm^{-1}, with a resolution of 4 cm^{-1} and 128 scans. Subsequently, they were deconvoluted using the Peakfit software and keeping the correlation coefficient (r^2) above 0.995. SEM was

carried out using JEOL JSM-6360 LV and FEI Quanta 200F microscopes using accelerating voltages from 15 to 20 kV. The samples used in these tests were embedded in epoxy resin, ground, and polished with diamond paste. Subsequently, the specimens were placed in an ultrasonic bath with acetone, dried under hot air, and sputter-coated with a 5 nm thick gold layer. Compositional analyses were performed using NORAN EDS systems available in the aforementioned microscopes.

μ-CT was carried out with a SKYSCAN 1172 high-resolution micro system. These tests were performed using an X-ray voltage tube of 100 kV and a 0.5 mm thick aluminum filter. A CCD camera with 2000 × 1048 pixels was used to record the transmission of the X-ray beam across the samples. Three-frame averaging and a rotation step of 0.30° were used, covering a view of 180°. Smoothing and beam-hardening correction were applied to suppress noise and beam hardening artifacts. The three-point flexural strength of the sintered samples was assessed using a mechanical testing stage available in the μ-CT system. These tests were performed as described in ASTM C1674-11. Samples with dimensions of about 5 mm × 5 mm × 15 mm were used in these tests. The flexural strength σ (MPa) of the examined materials was evaluated using equation (1):

$$\sigma = \frac{3Fl}{2bh^2}, \tag{1}$$

where F represents the critical load at fracture (N), l the distance between the two support pins (mm), b the sample width (mm), and h its height (mm).

3. RESULTS AND DISCUSSION

Figure 2 exhibits the XRD patterns of pure and TiO_2-containing alumina. The formation of β-Al_2TiO_5 was observed in the materials heat treated at either 1300 or 1500 °C because the formation of this phase usually occurs at temperatures above 1280 °C as per equation (2) [32]:

$$\alpha\text{-}Al_2O_3 + TiO_2 \rightarrow \beta\text{-}Al_2TiO_5 \ . \qquad (2)$$

However, the formation of β-Al_2TiO_5 was not easily seen at 1300 °C, though this phase was clearly observed in samples sintered at 1500 °C. These results strongly suggest that the driving force for the nucleation of β-Al_2TiO_5 is too small at 1300 °C, thus limiting its crystal growth. It is interesting to observe that the rutile phase is evident at 1100 and 1300 °C, but almost disappeared at 1500 °C. Therefore, the formation β-Al_2TiO_5 is associated with the transport of aluminum ions through rutile as reported elsewhere [32]. The XRD patterns exhibited in Figure 3 reveal that the intensity of the diffraction lines ascribed to β-Al_2TiO_5 increased when the concentration of TiO_2 also increased. By the same token, the intensity of the α-Al_2O_3 peaks decreased thus confirming that there was no reaction inhibition with increasing the amount of TiO_2. This behavior led to the shift of the reaction (2) to the right with an increased formation of β-Al_2TiO_5.

The FTIR spectra shown in Figure 4a are of similar shapes, displaying bands from 460 to 645 cm^{-1} which are ascribed to AlO_6 octahedra [33, 34]. The existence of these bands suggests that α-alumina is the major phase in these materials [35, 36]. This finding is in line with the results obtained by XRD (Figures 2 and 3). The bands ascribed to AlO_6

units are slightly shifted towards larger wavenumbers with the addition of TiO_2 to alumina, thus indicating the reaction of these two components. The bands at 780 cm^{-1} and 880 cm^{-1} is associated with AlO_4 units [37-39]. The band at 880 cm^{-1} is clearly observed in the spectrum of TiO_2-containing alumina calcined at 1500 °C, which is attributed to the presence of β-Al_2TiO_5 in this material. It was not possible to identify the bands related to Ti-O bonds because they are obscured by those associated with Al-O bonds. However, Figure 4b shows the results of the deconvoluted FTIR peaks, where the ratio of area of the peaks of 880cm^{-1}/650cm^{-1} increased almost linearly as a function of the TiO_2 loading. These results confirm the equimolar reaction in Equation (2), leading to the increased formation of the β-Al_2TiO_5 phase.

Figures 5A to 5C exhibit SEM micrographs of TiO_2-containing alumina calcined at 1500 °C, clearly showing the formation of dendritic pores. Figure 5D shows a schematic representation of a dendritic structure obtained during the freeze-casting technique and using camphene as the solvent. It is well established that the pore structure of freeze-cast materials is a direct replica of the solidified solvent structure [40-42]. As camphene tends to solidify in a dendritic fashion [43], its use as the solvent in freeze-casting gave rise to materials with dendritic pore channels [44-46]. It can be noticed from micrographs 5A to 5C that camphene dendrites grew macroscopically with a preferential orientation similar to the freezing direction, leading to elongated aligned pores and short secondary channels in the sintered body. Fast freezing rates such as that used in this work usually lead to fine pore structures in freeze-cast materials [47, 48].

Figure 6 depicts SEM micrograph and EDS spectra of TiO_2-containing alumina heat treated at 1500 °C. The dark-gray regions observed in this micrograph show EDS

signals ascribed to Al, whereas light-gray portions exhibited signals associated with Al and Ti. The latter is related to the existence of β-Al_2TiO_5 as its presence as small light-gray areas was dominated by large dark-gray areas. As the amount of Ti did not exceed 14 wt%, there is a good correlation between the areas allocated to β-Al_2TiO_5 and the high concentration of alumina (> 86 wt%). In addition, the light-gray areas are single domains enveloped by the alumina regions. Coupled with the XRD patterns in Figures 2 and 3, these results strongly indicate that alumina has reacted with Ti at discrete locations containing the rutile phase.

Figure 7 displays the porosity and shrinkage of samples as a function of the TiO_2 loading. The effect of the sintering temperature is clearly evidenced as higher values resulted in lowering the porosity and greater shrinkage of the samples. The initial increase of the TiO_2 loading from 0 to 4 wt% led to both an increase of the shrinkage and a decrease of the porosity. Nonetheless, a further addition of TiO_2 did not alter these properties. The Archimedes test also revealed that the materials obtained in this study show similar total and open porosities. This behavior suggests that they resulted in highly interconnected pore structures. Figure 8 exhibits the SEM micrographs of TiO_2-containing alumina calcined at 1500 °C. The heat treatment at this temperature led to materials with dense structures at the pore walls.

Figure 9 shows the three-point flexural strength of samples obtained in this study as a function of the TiO_2 loading. There was a slight increase in the flexural strength of samples heat treated at 1100 °C when the TiO_2 loading was increased. Samples calcined at 1300 °C showed a remarkable increase of their strength when the TiO_2 loading was changed from 0 to 1 wt%. The flexural strength of these materials remained nearly

constant when the TiO_2 loading was changed from 1 to 4 wt%. However, the increase of the TiO_2 loading from 4 to 7 wt% led to specimens with a higher flexural strength. A further addition of TiO_2 seems to decrease their strength. On one hand, materials calcined at 1500 °C showed a remarkable increase of their flexural strength when the TiO_2 loading was increased from 0 to 4 wt%. On the other hand, a further addition of TiO_2 slightly decreased their mechanical strength, though the results were within experimental variation. It is worth mentioning that, in spite of the high porosity of the samples used in this study, they withstood the flexural tests (up to fracture) and did not crumble upon handling.

Figure 10 shows μ-CT images of pure and TiO_2-containing alumina calcined at 1300 and 1500 °C. It was observed that the microstructure of TiO_2-containing samples heat treated at 1500 °C was significantly cracked. This behavior was not noticed for pure alumina or TiO_2-containing materials calcined at either 1100 or 1300 °C. A dense layer is clearly observed at the edges of the μ-CT image associated with pure alumina calcined at 1500 °C. These findings suggest that the presence of β-Al_2TiO_5 led to the formation of microcracks in titania-containing alumina.

As described in equation (2), β-Al_2TiO_5 usually forms in TiO_2-containing alumina at temperatures above 1280 °C. Thus, the formation of β-Al_2TiO_5 in samples heat treated at 1100 °C was unlikely. In this sense, the increase of the flexural strength of these samples when the TiO_2 loading was increased could be related to a more effective sintering of these samples (Figure 9). It has been reported that the addition of titania into alumina leads to an enhanced densification and grain growth [49-52]. Thus, the

increase of the flexural strength of materials calcined at 1100 °C could be related to the decrease of their porosity when the TiO_2 loading was increased.

The formation of β-Al_2O_3 is expected for materials calcined at either 1300 or 1500 °C. For samples heat treated at 1300 °C, the increase of the flexural strength when the TiO_2 loading was changed from 0 to 7 wt% could be associated with the formation of β-Al_2TiO_5 (Figure 9). Indeed, some researchers have reported that the addition of β-Al_2TiO_5 improved the fracture toughness of Al_2O_3 due to the increase of the residual stress ascribed to the mismatch of thermal expansion coefficient between α-Al_2O_3 and β-Al_2TiO_5 [53-55]. However, it must also be taken into consideration that the addition of TiO_2 could lead to an enhanced densification of Al_2O_3 (Figure 7) as reported elsewhere [49-52]. This behavior could also be contributing to the increase of the flexural strength in these specimens. The increase of the TiO_2 loading from 7 to 14 wt% led to samples with lower flexural strengths because a large amount of microcracks were formed in these materials. Thus, the loss of the mechanical strength of these specimens was related to the growth and propagation of cracks. This behavior has already been reported for highly microcracked TiO_2-Al_2O_3 samples [56, 57]. It is well established that aluminum titanate exhibits an anisotropic thermal expansion along the three primary axes of the crystal lattice, which leads to the formation of microcracks [58, 59].

The effect of the growth and propagation of microcracks seems to be more pronounced in samples heat treated at 1500 °C. It was observed that these materials showed a loss of mechanical strength when TiO_2 loadings above 4 wt% were used in their synthesis.

Figure 11 exhibits the flexural strength and β-Al_2TiO_5 concentration for samples prepared with different TiO_2 loadings and heat treated at 1500 °C. The concentration of β-Al_2TiO_5 was evaluated using the XPert Plus software. It can be noticed that the higher the TiO_2 loading, the larger the concentration of β-Al_2TiO_5. It is observed by plotting the flexural strength as a function of the β-Al_2TiO_5 concentration that it tends to decrease for high concentrations of aluminum titanate. It is worth noting that this curve and that shown in Figure 9 exhibit a similar shape. These results strongly suggest that a high concentration of microcracks could be present in the specimens containing TiO_2 loadings above 4 wt%. This scenario led to decreasing the mechanical strength of these samples. As shown in Figure 10, μ-CT revealed a significant concentration of cracks in the microstructure of TiO_2-containing sample heat treated at 1500 °C.

Finally, Figure 12 displays the flexural strength of samples prepared using different TiO_2 loadings as a function of the porosity. It is observed that for samples obtained with loadings below 4 wt%, the higher the sintering temperature, the larger the flexural strength. Nonetheless, this behavior was not observed for materials prepared using TiO_2 loadings above 7 wt%; they showed similar flexural strengths when heat treated at either 1300 or 1500 °C. It is interesting to note that although the porosity decreased, the flexural strength remained almost constant. This find is counterintuitive as it would be expected an increase in flexural strength as the material densifies as the porosity decreased. This finding is related to the existence of β-Al_2TiO_5 in the microstructure of these specimens coupled with the microcracks resultant at sintering at 1500 °C.

4. CONCLUSIONS

XRD revealed that the formation of β-Al_2TiO_5 in materials heat treated at temperatures above 1300 °C. The loading of TiO_2 into α-Al_2O_3 resulted in more pronounced XRD peaks ascribed to β-Al_2TiO_5. Features assigned to α-Al_2O_3 were clearly observed in the FTIR spectra thus confirming that α-Al_2O_3 is the major phase in these materials, which is in agreement with the results obtained by XRD. Dendritic pores associated with the effect of the solvent camphene grew macroscopically with a preferential orientation similar to the freezing direction, leading to elongated aligned pores and short secondary channels in the sintered body. Light-gray regions with EDS signals related to Al and Ti were attributed to β-Al_2TiO_5.

Samples calcined at 1100 °C showed a slight increase of their flexural strength when the TiO_2 loading was increased that stemmed from the occurrence of a more effective sintering of alumina. Samples heat treated at either 1300 or 1500 °C showed an initial increase of their flexural strength with increasing the TiO_2 loading, followed by a loss of mechanical strength for TiO_2 loadings in excess of 4 wt%. Even though the materials became denser with loss of porosity, the reduced mechanical strength was attributed to the formation of microcracks in the microstructure which increased as a function of the TiO_2 loading. The findings described in this work point out that a small addition of TiO_2 can optimize the mechanical strength of freeze-cast alumina samples.

ACKNOWLEDGMENTS

The authors thank the financial support from FAPEMIG, CAPES, and CNPq. We also appreciate Dra. Andréia Bicalho and UFMG microscopy center for the technical support in the XRD and SEM tests, respectively. The authors are grateful to Almatis Brasil for providing the alumina powder used in this work. J.C. Diniz da Costa acknowledges the support given by the Australian Research Council (ARC) Future Fellowship Program (FT130100405).

REFERENCES

[1] I.K. Jun, Y.H. Koh, J.H. Song, S.H. Lee, H.E. Kim, Improved compressive strength of reticulated porous zirconia using carbon coated polymeric sponge as novel template, Mater. Lett. 60 (2006) 2507-2510.

[2] G. Plesch, M. Gorbar, U.F. Vogt, K. Jesenak, M. Vargova, Reticulated macroporous ceramic foam supported TiO_2 for photocatalytic applications, Mater. Lett. 63 (2009) 461-463.

[3] C. Tuck, J.R.G. Evans, Porous ceramics prepared from aqueous foams, J. Mater. Sci. Lett. 18 (1996) 1003-1005.

[4] S. Barg, D. Koch, G. Grathwohl, Processing and properties of graded ceramic filters, J. Am. Ceram. Soc. 92 (2009) 2854-2860.

[5] H. Schmidt, D. Koch, G. Grathwohl, Micro/macro-porous ceramics from preceramic precursors, J. Am. Ceram. Soc. 84 (2005) 2252-2255.

[6] M. Wilhelm, M. Adam, M. Bäumer, G. Grathwohl, Synthesis and properties of porous hybrid materials containing metallic nanoparticles, Adv. Eng. Mater. 10 (2008) 241-245.

[7] O. Lyckfeldt, J.M.F. Ferreira, Processing of porous ceramics by starch consolidation, J. Eur. Ceram. Soc. 18 (1998) 131-140.

[8] P. Colombo, E. Bernardo, Macro- and micro-cellular porous ceramics from preceramic polymers, Compos. Sci. Technol. 63 (2003) 2353-2359.

[9] L. Qian, H. Zhang, Controlled freezing and freeze drying: A versatile route for porous and micro-/nano-structured materials, J. Chem. Technol. Biotechnol. 86 (2011) 172-184.

[10] S. Deville, Freeze-casting of porous ceramics: A review of current achievements and issues, Adv. Eng. Mater. 10 (2008) 154-169.

[11] S. Deville, Freeze-casting of porous biomaterials: Structure, properties and opportunities, Materials. 3 (2010) 1913-1927.

[12] X.W. Zhu, D.L. Jiang, S.H. Tan, Z.Q. Zhang, Improvement in the strut thickness of reticulated porous ceramics, J. Am. Ceram. Soc. 84 (2001) 1654-1656.

[13] K. Araki, J.W. Halloran, Porous ceramic bodies with interconnected pore channels by a novel freeze casting technique, J. Am. Ceram. Soc. 88 (2005) 1108-1114.

[14] S. Deville, E. Saiz, A. Tomsia, Freeze casting of hydroxyapatite scaffolds for bone tissue engineering, Biomaterials. 27 (2006) 5480-5489.

[15] U.G.K. Wegst, M. Schecter, A.E. Donius, P.M. Hunger, Biomaterials by freeze casting, Phil. Trans. R. Soc. A. 368 (2010) 2099-2121.

[16] L. Estevez, A. Kelarakis, Q. Gong, E.H. Da'as, E.P. Giannelis, Multifunctional graphene/platinum/nafion hybrids via ice templating, J. Am. Chem. Soc. 133 (2011) 6122-6125.

[17] J. Kuang, L. Liu, Y. Gao, D. Zhou, Z. Chen, B. Han, Z. Zhang, A hierarchically structured graphene foam and its potential as a large-scale strain-gauge sensor, Nanoscale. 5 (2013) 12171-12177.

[18] A. Szepes, J. Ulrich, Z. Farkas, J. Kovács, P. Szabó-Révész, Freeze-casting technique in the development of solid drug delivery systems, Chem. Eng. Process. Process Intensif. 46 (2007) 230-238.

[19] J.S. Son, M. Appleford, J.L. Ong, J.C. Wenke, J.M. Kim, S.H. Choi, Porous hydroxyapatite scaffold with three-dimensional localized drug delivery system using biodegradable microspheres, J. Controlled Release. 153 (2011) 133-140.

[20] Z.-Y. Deng, H.R. Fernandes, J.M. Ventura, S. Kannan, J.M.F. Ferreira, Nano-TiO_2-coated unidirectional porous glass structure prepared by freeze drying and solution infiltration, J. Am. Ceram. Soc. 90 (2007) 1265-1268.

[21] Z. Xing, J. Li, Q. Wang, W. Zhou, G. Tian, K. Pan, C. Tian, J. Zou, H. Fu, A floating porous crystalline TiO_2 ceramic with enhanced photocatalytic performance for wastewater decontamination, Eur. J. Inorg. Chem. 2013 (2013) 2411-2417.

[22] S.W. Sofie, Fabrication of functionally graded and aligned porosity in thin ceramic substrates with the novel freeze-tape-casting process, J. Am. Ceram. Soc. 90 (2007) 2024-2031.

[23] A. Ojuva, F. Akhtar, A.P. Tomsia, L. Bergström, Laminated adsorbents with very rapid CO_2 uptake by freeze-casting of zeolites, ACS Appl. Mater. Interfaces. 5 (2013) 2669-2676.

[24] D.F. Souza, E.H.M. Nunes, D.S. Pimenta, D.C.L. Vasconcelos, J.F. Nascimento, W. Grava, M. Houmard, W.L. Vasconcelos, Synthesis and structural evaluation of freeze-cast porous alumina, Mater. Charact. 96 (2014) 183-195.

[25] A. Gutiérrez-Alejandrea, M. González-Cruza, M. Trombettab, G. Buscab, J. Ramírez, Characterization of alumina-titania mixed oxide supports: Part II: Al_2O_3-based supports, Microporous Mesoporous Mater. 23 (1998) 265-275.

[26] W. Lin, Y.X. Zhu, N.Z. Wu, Y.C. Xie, I. Murwani, E. Kemnitz, Total oxidation of methane at low temperature over $Pd/TiO_2/Al_2O_3$: Effects of the support and residual chlorine ions, Appl. Catal. B. 50 (2004) 59-66.

[27] B. Ferrari, A. Bartret, C. Baudín, Sandwich materials formed by thick alumina tapes and thin-layered alumina-aluminium titanate structures shaped by EPD, J. Eur. Ceram. Soc. 29 (2009) 1083-1092.

[28] P. Fauchais, G. Montavon, R.S. Lima, B.R. Marple, Engineering a new class of thermal spray nano-based microstructures from agglomerated nanostructured particles, suspensions and solutions: An invited review, J. Phys. D: Appl. Phys. 44 (2011) 1-53.

[29] A. Kebbede, J. Parai, A.H. Carim, Anisotropic grain growth in α-Al_2O_3 with SiO_2 and TiO_2 additions, J. Am. Ceram. Soc. 83 (2000) 2845-2851.

[30] S.W. Lee, C. Morillo, J. Lira-Olivares, S.H. Kim, T. Sekino, K. Niihara, B.J. Hockey, Tribological and microstructural analysis of Al_2O_3/TiO_2 nanocomposites to use in the femoral head of hip replacement, Wear. 255 (2003) 1040-1044.

[31] P. Ctibor, L. Kraus, J. Tuominen, P. Vuoristo, P. Chráska, Improvement of mechanical properties of alumina and zirconia plasma sprayed coatings induced by laser post-treatment, Ceram. Silik. 51 (2007) 181-189.

[32] V. Buscaglia, M. Alvazzi Delfrate, M. Leoni, C. Bottino, P. Nanni, The effect of $MgAl_2O_4$ on the formation kinetics of Al_2TiO_5 from Al_2O_3 and TiO_2 fine powders, J. Mater. Sci. 31 (1996) 1715-1724.

[33] H. Joe, A.K. Vasudevan, G. Aruldhas, A.D. Damodaran, K.G.K. Warrier, FTIR as a tool to study high-temperature phase formation in sol-gel aluminium titanate, J. Solid State Chem. 131 (1997) 181-184.

[34] A. Adamczyk, E. Długon, The FTIR studies of gels and thin films of Al_2O_3-TiO_2 and Al_2O_3-TiO_2-SiO_2 systems, Spectrochim. Acta Part A. 89 (2012) 11-17.

[35] A.R. Garcia, R.B. de Barros, A. Fidalgo, L.M. Ilharco, Interactions of L-alanine with alumina as studied by vibrational spectroscopy, Langmuir. 23 (2007) 10164-10175.

[36] C. Morterra, G. Magnacca, A case study: Surface chemistry and surface structure of catalytic aluminas, as studied by vibrational spectroscopy of adsorbed species, Catal. Today. 27 (1996) 497-532.

[37] P. Tarte, Infrared spectra of inorganic aluminates and characteristic vibrational frequencies of AlO_4 tetrahedra and AlO_6 octaedra, Spectrochim. Acta Part A. 23 (1967) 2127-2143.

[38] M. Crişan, M. Zaharescu, V.D. Kumari, M. Subrahmanyam, D. Crişan, N. Drăgan, M. Răileanu, M. Jitianu, A. Rusu, G. Sadanandam, J.K.Reddy, Sol-gel based alumina powders with catalytic applications, Appl. Surf. Sci. 258 (2011) 448-455.

[39] F.I. Hurwitz, H. Guo, R.B. Rogers, E.J. Sheets, D.R. Miller, K.N. Newlin, M.K. Shave, A.R. Palczer, M.T. Cox, Influence of Ti addition on boehmite-derived aluminum silicate aerogels: Structure and properties, J. Sol-Gel Sci. Technol. 64 (2012) 367-374.

[40] C. Hong, X. Zhang, J. Han, J. Du, W. Han, Ultra-high-porosity zirconia ceramics fabricated by novel room-temperature freeze-casting, Scr. Mater. 60 (2009) 563-566.

[41] M.P. Ginebra, M. Espanol, E.B. Montufar, R.A. Perez, G. Mestres, New processing approaches in calcium phosphate cements and their applications in regenerative medicine, Acta Biomater. 6 (2010) 2863-2873.

[42] Y. Zhou, S. Fu, Y. Pu, S. Pan, M.V. Levitb, A.J. Ragauskas, Freeze-casting of cellulose nanowhisker foams prepared from a water-dimethylsulfoxide (DMSO) binary mixture at low DMSO concentrations, RSC Adv. 3 (2013) 19272-19277.

[43] A. Macchetta, I.G. Turner, C.R. Bowen, Fabrication of HA/TCP scaffolds with a graded and porous structure using a camphene-based freeze-casting method, Acta Biomater. 5 (2009) 1319-1327.

[44] K. Araki, J.W. Halloran, Room-temperature freeze casting for ceramics with nonaqueous sublimable vehicles in the naphthalene-camphor eutectic system, J. Am. Ceram. Soc. 87 (2004) 2014-2019.

[45] J. Han, C. Hong, X. Zhang, J. Du, W. Zhang, Highly porous ZrO_2 ceramics fabricated by a camphene-based freeze-casting route: Microstructure and properties, J. Eur. Ceram. Soc. 30 (2010) 53-60.

[46] E.C. Hammel, O.L.-R. Ighodaro, O.I. Okoli, Processing and properties of advanced porous ceramics: An application based review, Ceram. Int. 40 (2014) 15351-15370.

[47] E.R. Rubinstein, M.E. Glicksman, Dendritic growth kinetics and structure II. Camphene, J. Cryst. Growth. 112 (1991) 97-110.

[48] W.L. Li, K. Lu, J.Y. Walz, Freeze casting of porous materials: review of critical factors in microstructure evolution, Int. Mater. Rev. 57 (2012) 37-60.

[49] H.P. Cahoon, C.J. Christensen, Sintering and grain growth of alpha-alumina, J. Am. Ceram. Soc. 39 (1956) 337-344.

[50] G. Rossi, J.E. Burke, Influence of additives on the microstructure of sintered Al_2O_3, J. Am. Ceram. Soc. 56 (1973) 654-659.

[51] Y.-M. Kim, S.-H.Hong, D.-Y. Kim, Anisotropic abnormal grain growth in TiO_2/SiO_2-doped alumina, J. Am. Ceram. Soc. 83 (2000) 2809-2812.

[52] R.D. Bagley, I.B. Cutler, D.L. Johnson, Effect of TiO_2 on initial sintering of Al_2O_3, J. Am. Ceram. Soc. 53 (1970) 136-141.

[53] N.P. Padture, S.J. Bennison, H.M. Chan, Model for toughness curves in two-phase ceramics: II Microstructural variables, J. Am. Ceram. Soc. 76 (1993) 2312-2320.

[54] S. Bueno, M.H. Berger, R. Moreno, C. Baudín, Fracture behaviour of microcrack-free alumina-aluminium titanate ceramics with second phase nanoparticles at alumina grain boundaries, J. Eur. Ceram. Soc. 28 (2008) 1961-1971.

[55] S. Bueno, M.G. Hernández, T. Sánchez, J.J. Anaya, C. Baudín, Non-destructive characterisation of alumina/aluminium titanate composites using a micromechanical model and ultrasonic determinations: Part I. Evaluation of the effective elastic constants of aluminium titanate, Ceram. Int. 34 (2008) 181-188.

[56] L.A. Stanciu, J.R. Groza, V.Y. Kodash, Electric-field effects on sintering and reaction to form aluminum titanate from binary alumina-titania sol-gel powders, J. Am. Ceram. Soc. 84 (2001) 983-985.

[57] T.L. Lekanova, Y.I. Ryabkov, O.A. Sevbo, V.V. Viktorov, Phase relations in the systems Al_2TiO_5-Fe_2O_3, Al_2O_3-TiO_2-Fe_2O_3, and Al_2TiO_5-Cr_2O_3, Inorg. Mater. 40 (2004) 1191-1195.

[58] B. Morosin, R.W. Lynch, Structure studies on Al_2TiO_5 at room temperature and at 600 °C, Acta Crystallogr. B: Struct. Sci. B28 (1972) 1040-1046.

[59] I.B. de Arenas, Reactive sintering of aluminum titanate, in: A. Lakshmanan (Ed.), Sintering of ceramics - New emerging techniques, InTech, Rijeka (Croatia), 2012, pp. 501-526.

FIGURE CAPTIONS

- Figure 1: Schematic of the steps used in this work for samples preparation.

- Figure 2: XRD patterns of pure and TiO_2-containing alumina heat treated at different temperatures. The JCPDS file numbers 00-021-1272, 00-021-1276, 00-041-0258, and 00-010-0173 were used as reference for anatase, rutile, β-Al_2TiO_5, and α-Al_2O_3, respectively.

- Figure 3: XRD patterns of samples prepared using different concentrations of TiO_2. Materials heat treated at 1500 °C. The JCPDS file numbers 00-021-1272, 00-021-1276, 00-041-0258, and 00-010-0173 were used as reference for anatase, rutile, β-Al_2TiO_5, and α-Al_2O_3, respectively.

- **Figure 4:** (a) FTIR spectra of pure and TiO_2-containing alumina heat treated at different temperatures. The spectra were normalized using the band at 645 cm^{-1} as reference. (b) Deconvolution of the FTIR spectra of samples calcined at 1500 °C.

- Figure 5: (A-C) SEM micrographs of TiO_2-containing alumina calcined at 1500 °C. (D) Schematic representation of dendritic pore structure observed in freeze-cast material prepared using camphene as the solvent. The scale bars correspond to 100, 50, and 10 μm in (A), (B), and (C), respectively. SEM micrographs obtained using secondary electrons as the imaging signal.

- **Figure 6:** SEM micrograph and EDS spectra of TiO_2-containing alumina heat treated at 1500 °C. The scale bar in the micrograph corresponds to 10 μm. SEM micrograph obtained using backscattered electrons as the imaging signal. The EDS signal ascribed to C is associated with the epoxy resin in which samples were embedded before the SEM tests.

- **Figure 7:** Porosity and shrinkage of samples prepared in this work as a function of the TiO_2 loading. The dotted lines are used only as a guide to the eyes.

- **Figure 8:** SEM micrographs of TiO_2-containing alumina heat treated at 1500 °C.

- **Figure 9:** Three-point flexural strength of samples prepared using different TiO_2 loadings. The dotted lines are used only as a guide to the eyes.

- **Figure 10:** μ-CT images of pure and TiO_2-containing alumina calcined at either 1300 or 1500 °C. The white and gray regions represent the solid phase.

- **Figure 11:** Flexural strength and β-Al_2TiO_5 concentration for samples prepared using different TiO_2 loadings and heat treated at 1500 °C.

- **Figure 12:** Flexural strength of samples prepared using different TiO_2 loadings as a function of the porosity.

Figure 1

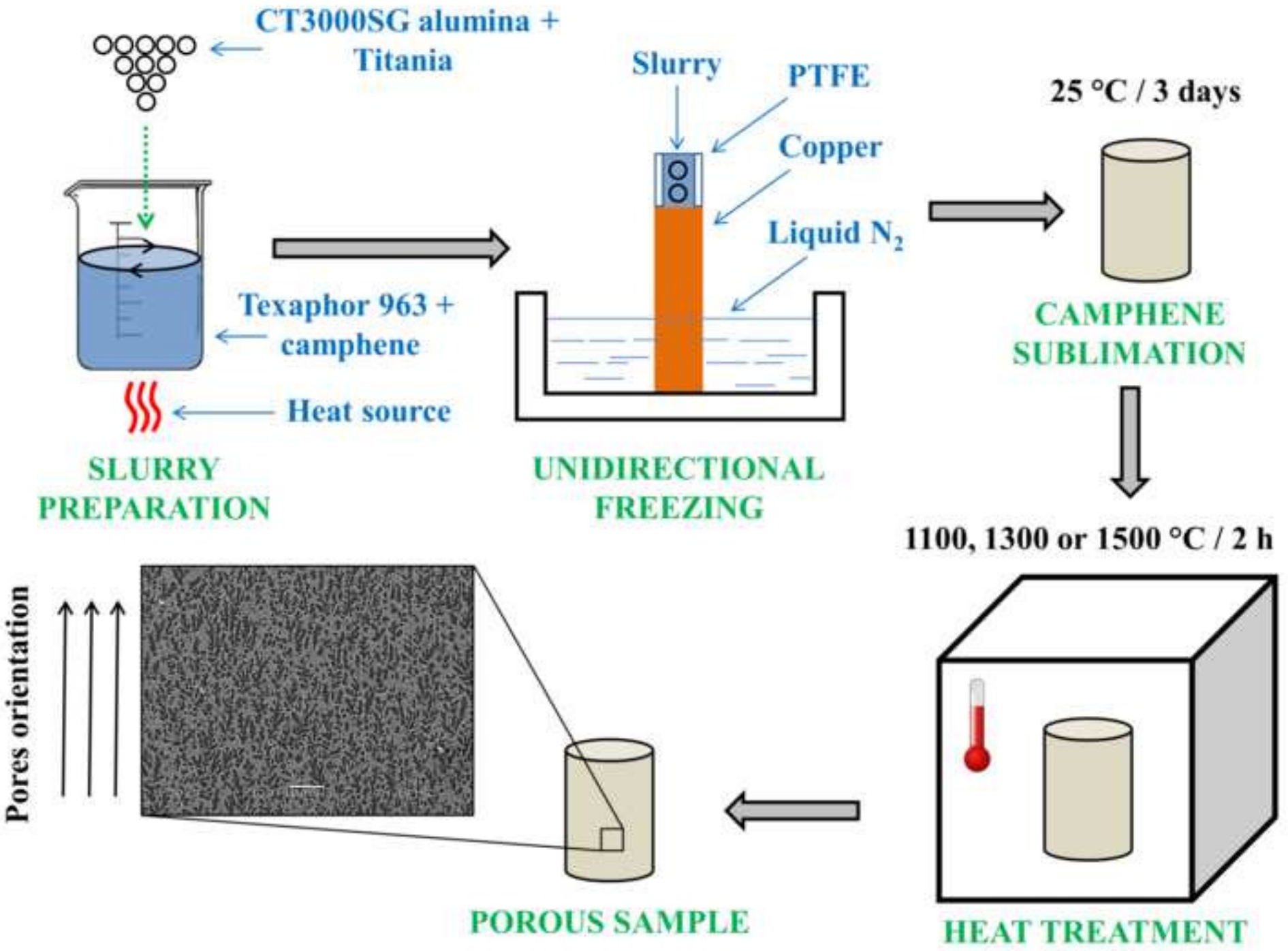

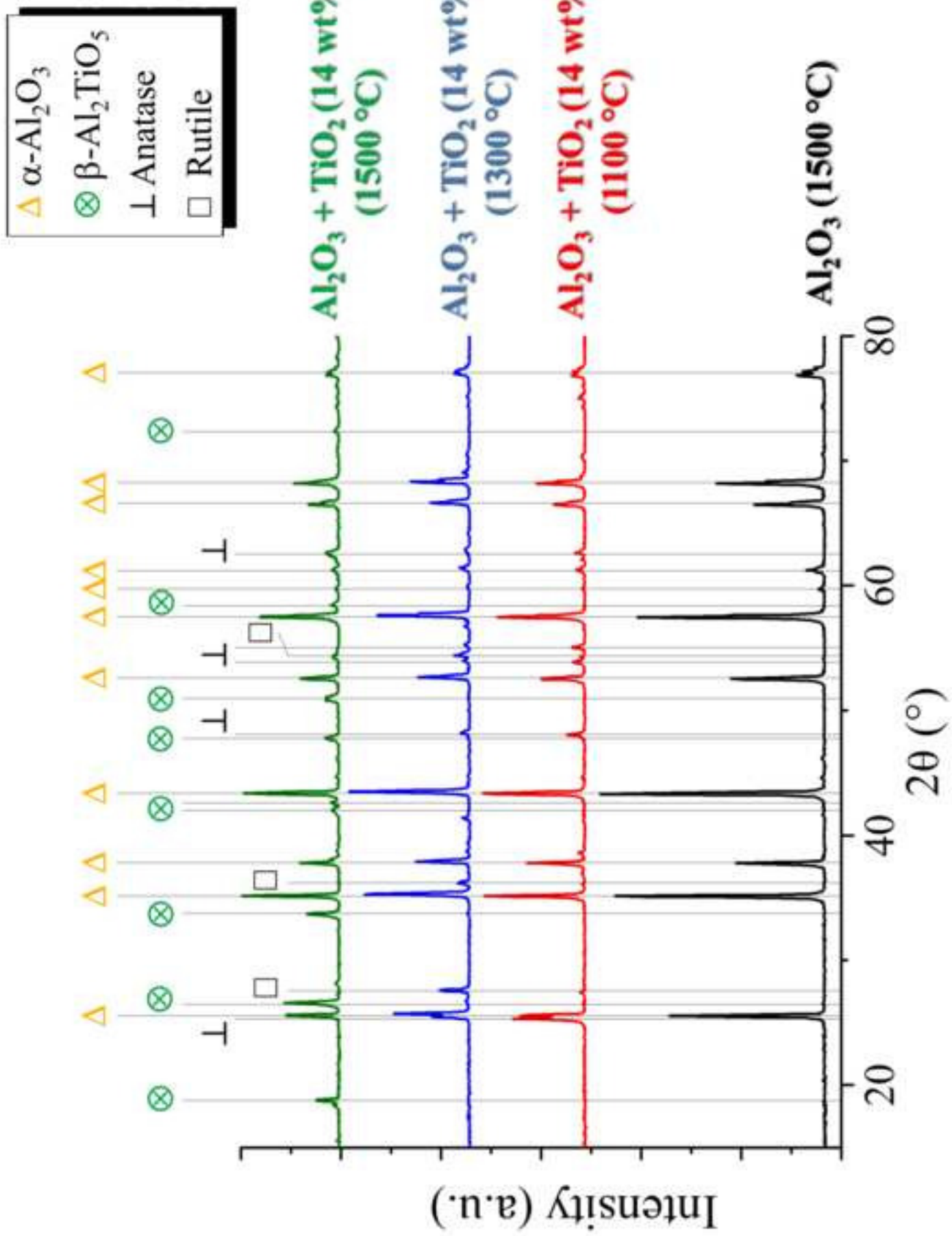

Figure 2

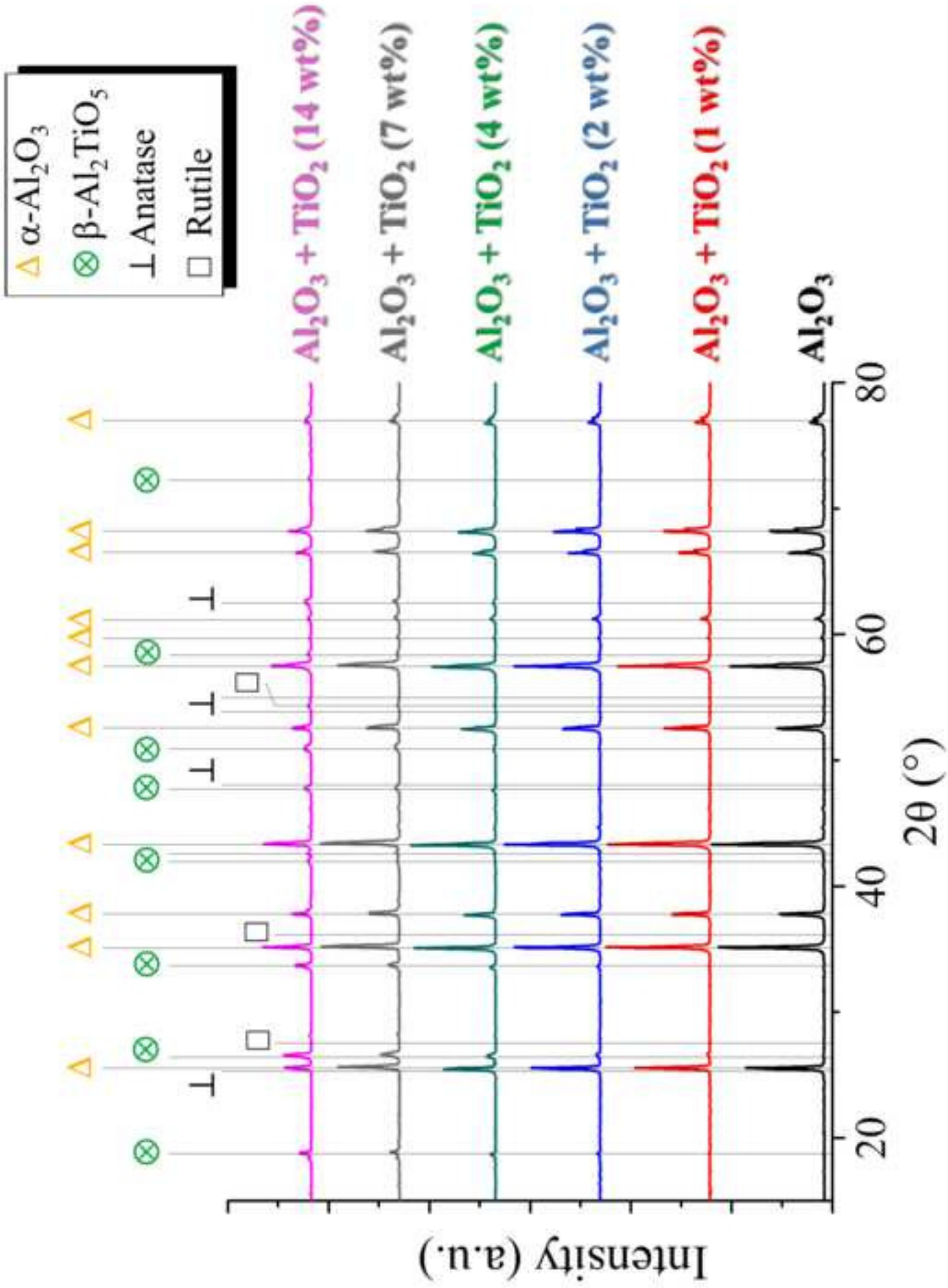
α-Al2O3
β-Al2TiO5
Anatase
Rutile
Al2O3 + TiO2 (14 wt%)
Al2O3 + TiO2 (7 wt%)
Al2O3 + TiO2 (4 wt%)
Al2O3 + TiO2 (2 wt%)
Al2O3 + TiO2 (1 wt%)
Al2O3
Intensity (a.u.)
2θ (°)
20
40
60
80

Figure 3

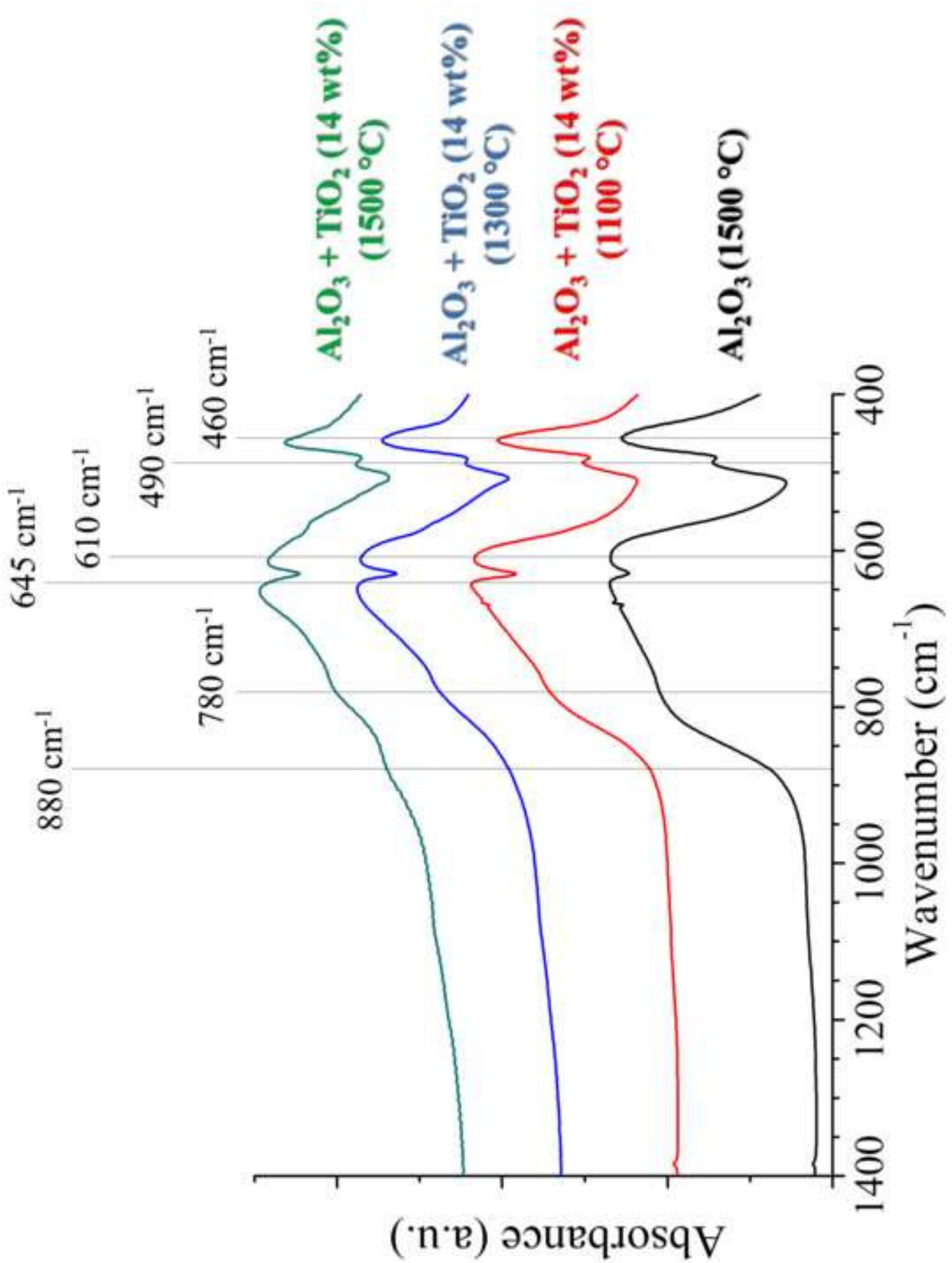
Al2O3 + TiO2 (14 wt%) (1500 °C)
Al2O3 + TiO2 (14 wt%) (1300 °C)
Al2O3 + TiO2 (14 wt%) (1100 °C)
Al2O3 (1500 °C)
880 cm-1
780 cm-1
645 cm-1
610 cm-1
490 cm-1
460 cm-1
Absorbance (a.u.)
Wavenumber (cm-1)
1400
1200
1000
800
600
400

Figure 4a

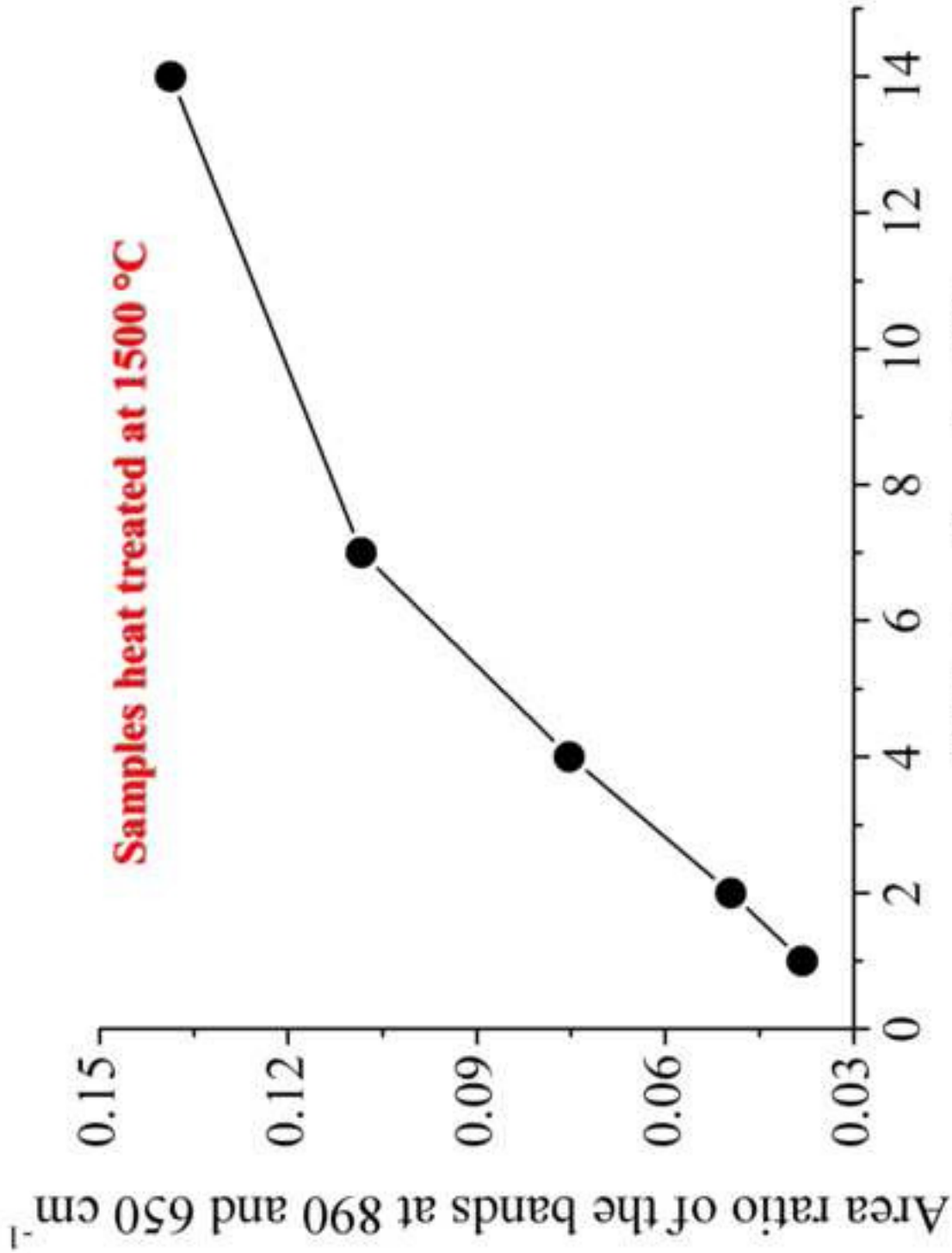
Samples heat treated at 1500 °C
Area ratio of the bands at 890 and 650 cm-1
TiO2 loading (wt%)
0.03
0.06
0.09
0.12
0.15
0
2
4
6
8
10
12
14

Figure 4b

Figure 5

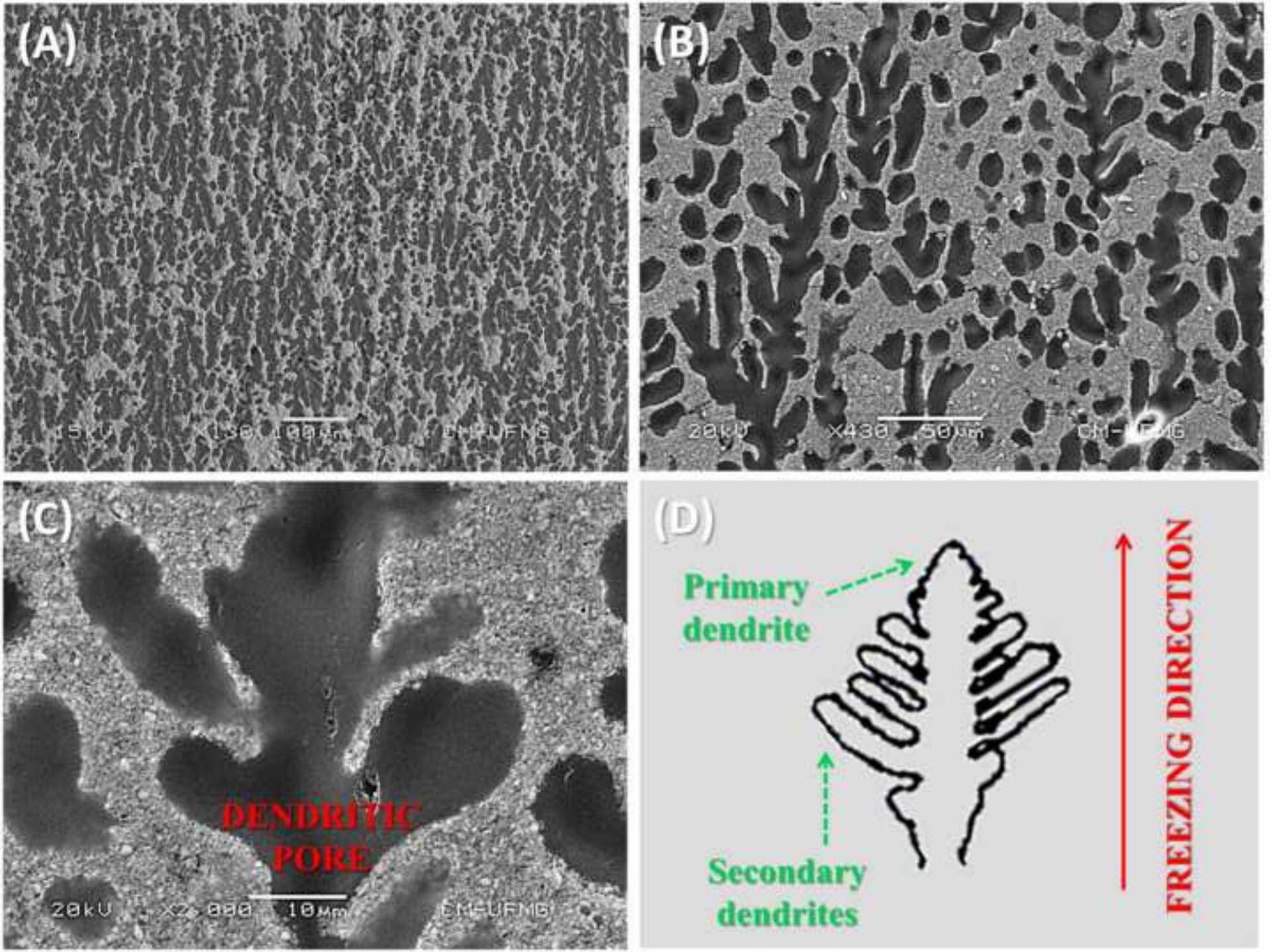

Figure 6

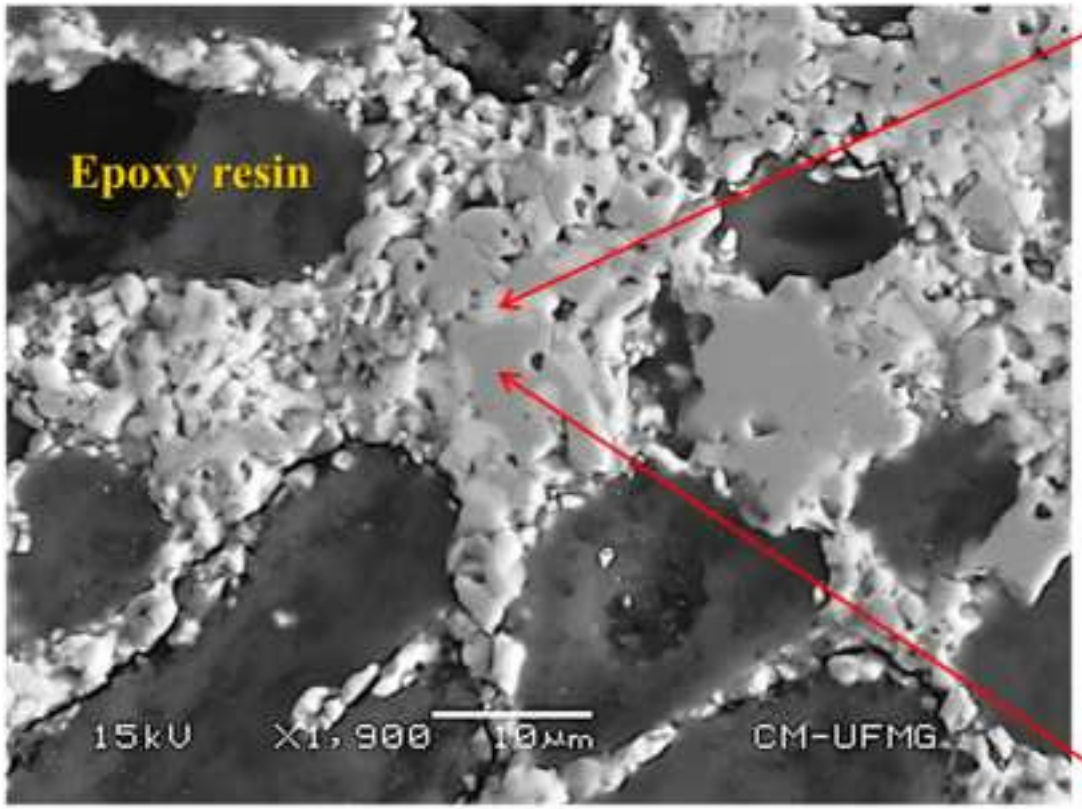

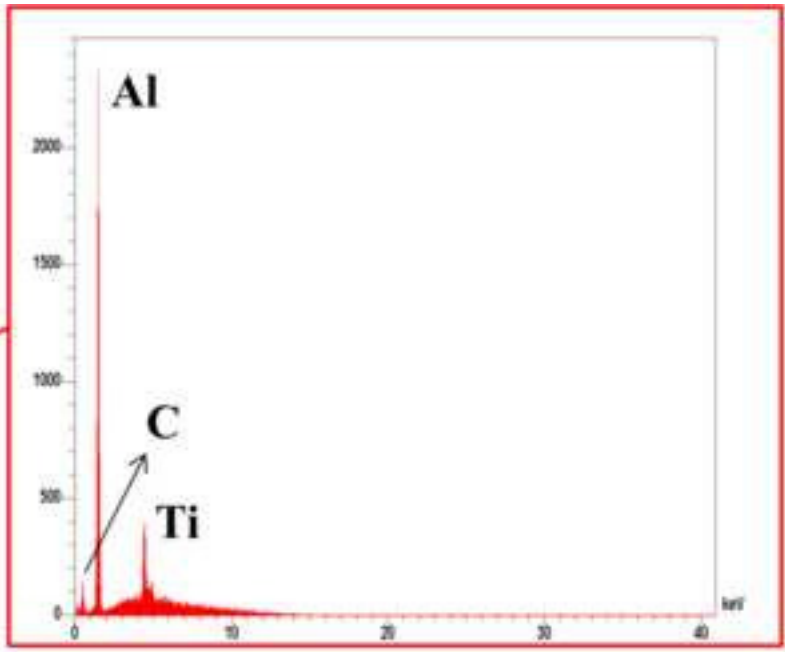

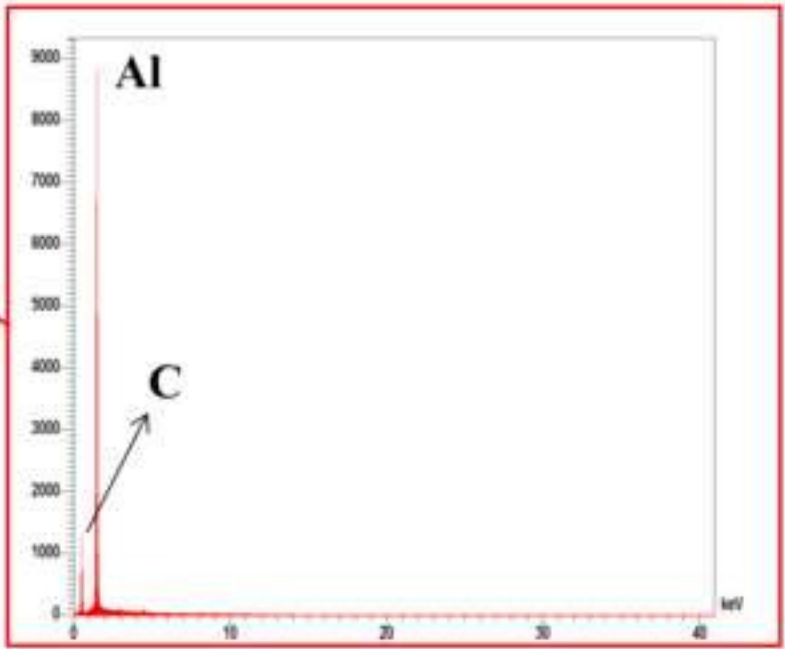

Figure 7

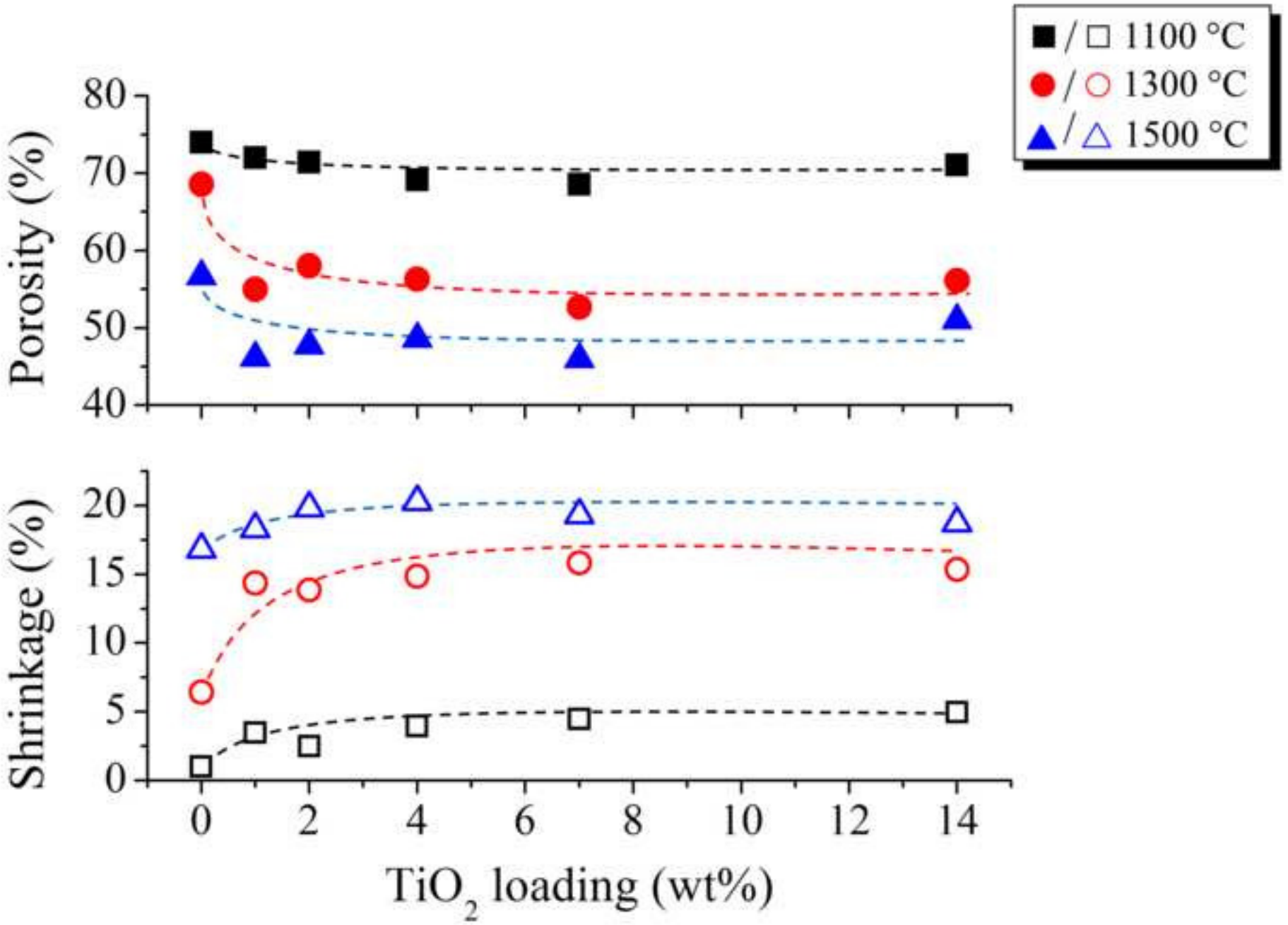

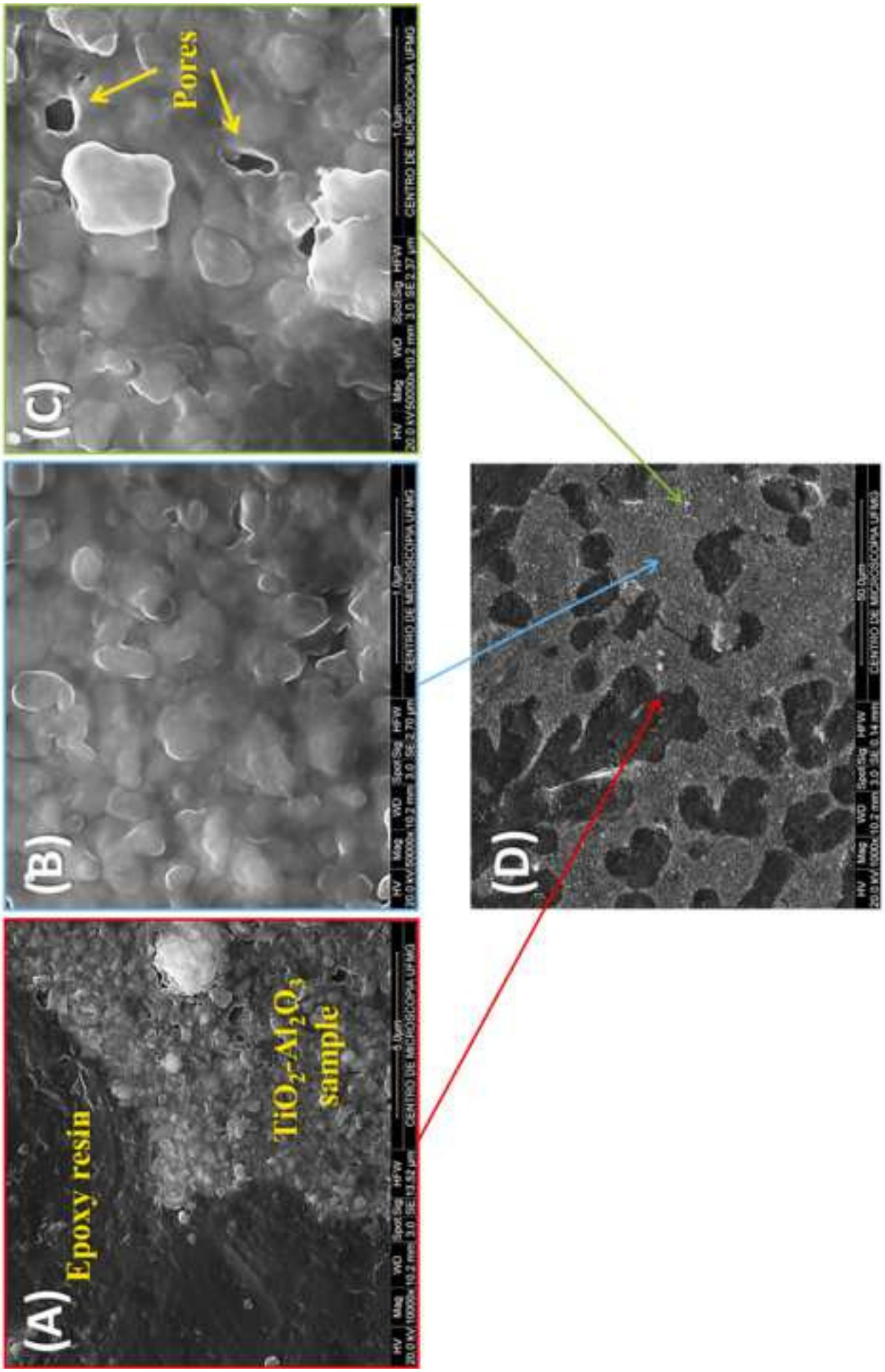

Figure 8

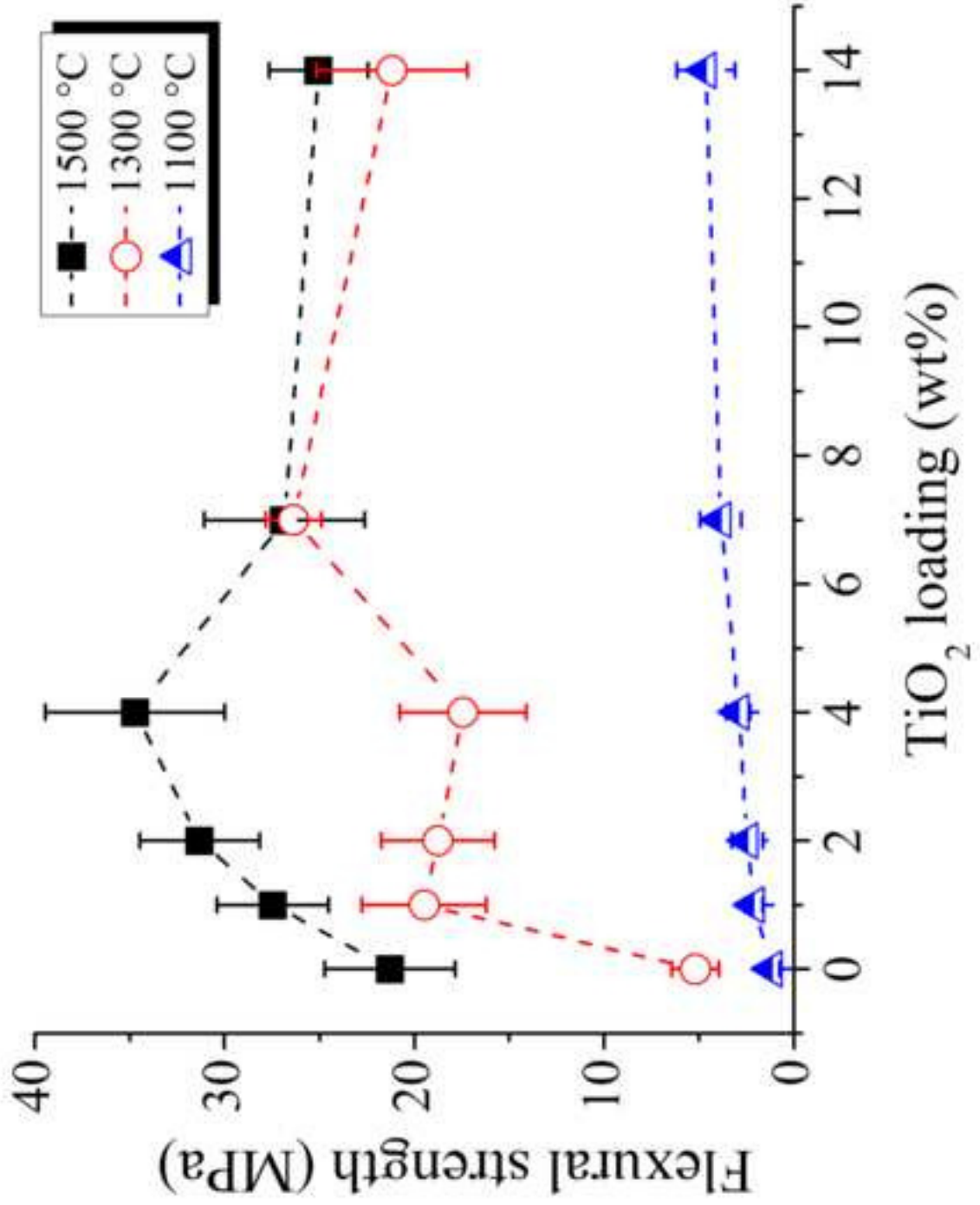
1500 °C
1300 °C
1100 °C
Flexural strength (MPa)
0
10
20
30
40
0
2
4
6
8
10
12
14
TiO2 loading (wt%)

Figure 9

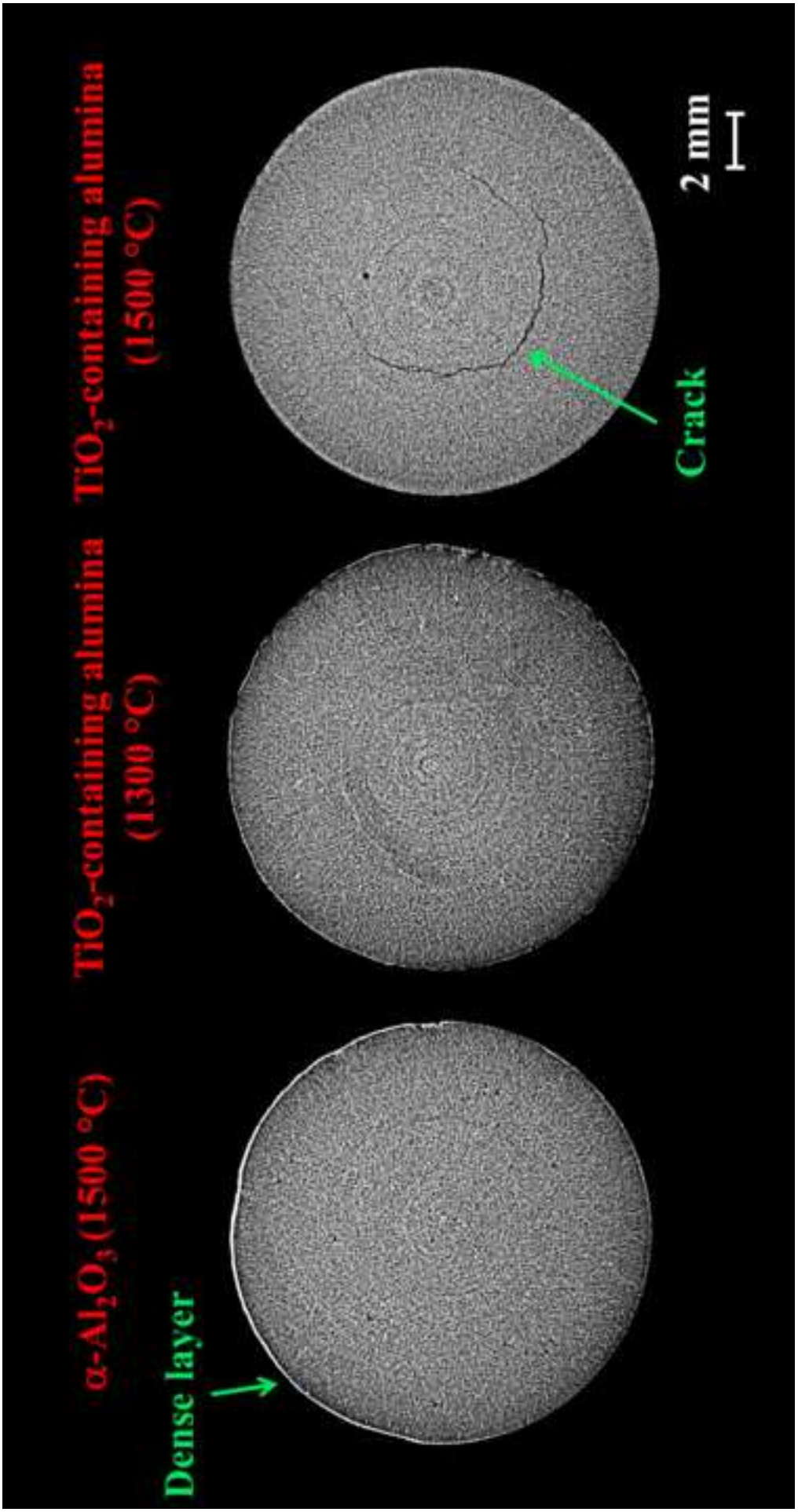
α-Al2O3 (1500 °C)
TiO2-containing alumina (1300 °C)
TiO2-containing alumina (1500 °C)
Dense layer
Crack
2 mm

Figure 10

Figure 11

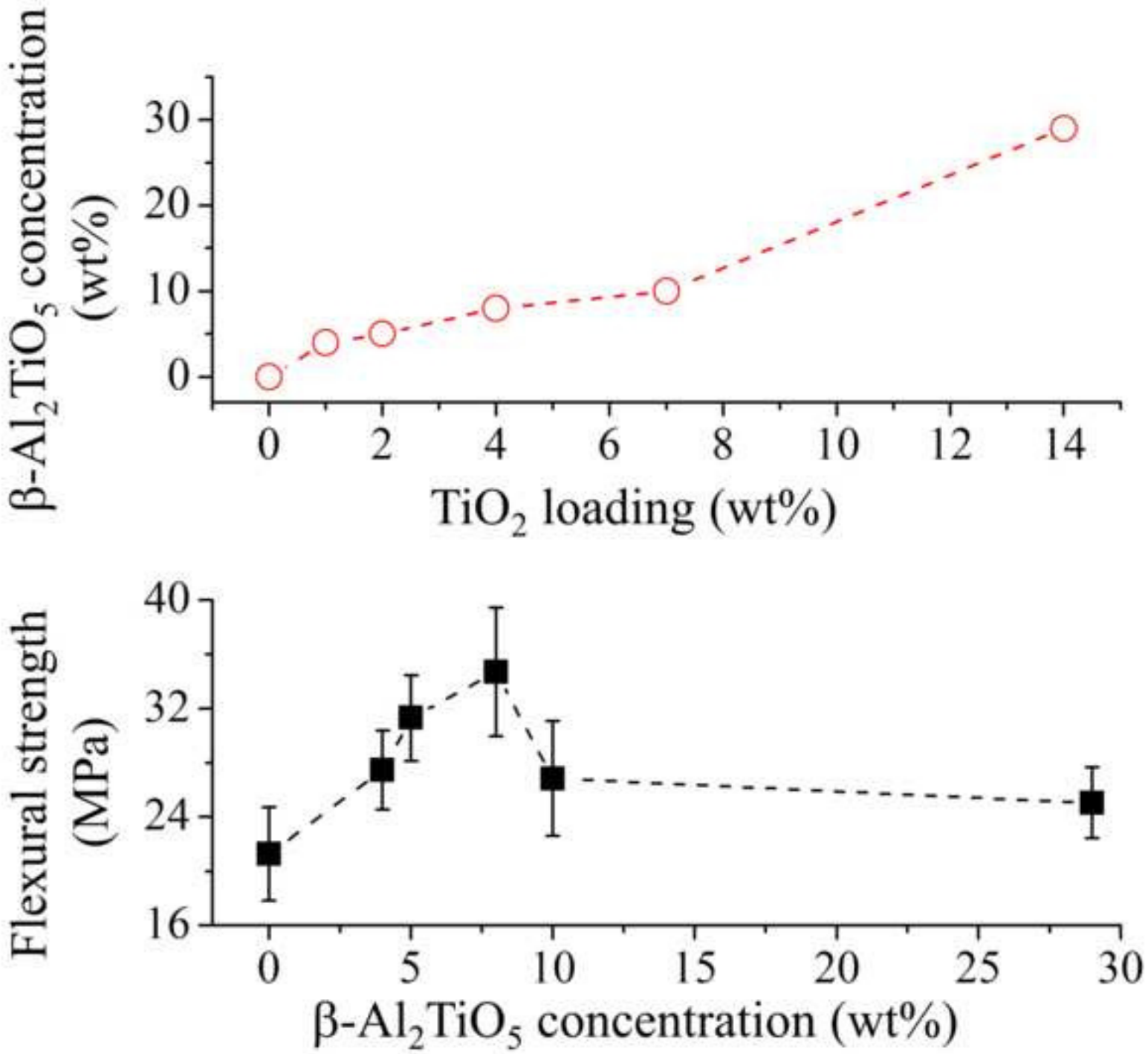

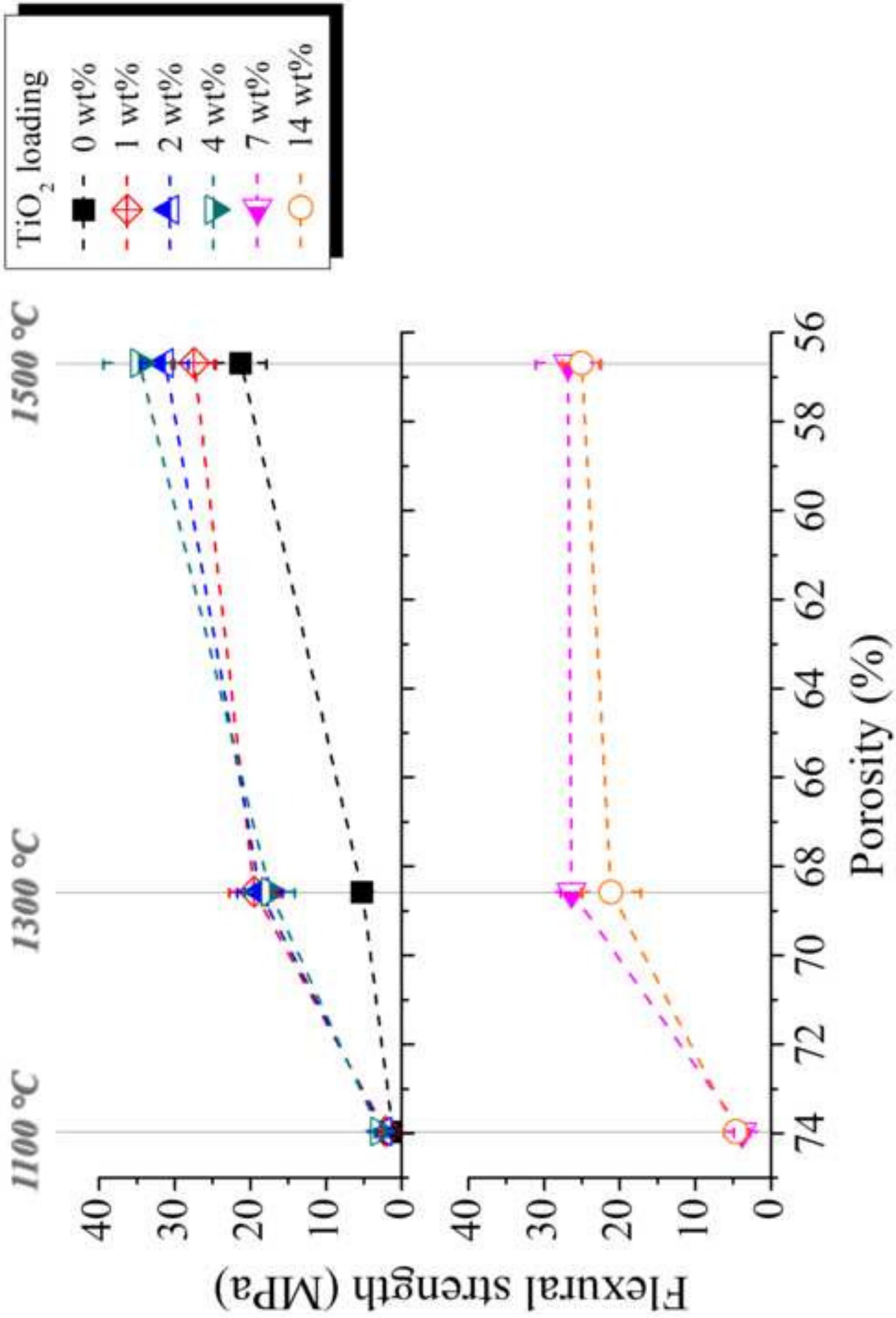
TiO2 loading
0 wt%
1 wt%
2 wt%
4 wt%
7 wt%
14 wt%
1100 °C
1300 °C
1500 °C
Flexural strength (MPa)
Porosity (%)
0
10
20
30
40
74
72
70
68
66
64
62
60
58
56

Figure 12